# Solid-State Electronic Conductivity Studies of Monolayer Protected Au Clusters

*A Summary Report to The Electrochemical Society for the 2000 Edward G. Weston Summer Research Fellowship*

**by W. Peter Wuelfing**

Our lab is interested in the solid-state electronic conductivity of a specific type of metallic nanoparticle (dubbed Monolayer Protected Gold Clusters—MPCs)[1] and has pursued their early development as useful electronic components during this summer fellowship period. Initial work on this subject revealed that the charge transport mechanism in MPC films was electron-tunneling from Au core to Au core through alkanethiolate chains with an electron tunneling coefficient, β, of 1.2 $Å^{-1}$.[2] This was determined by collecting current-voltage data on a series of variable alkanethiolate MPCs that were drop-cast and vacuum dried on interdigitated array electrodes of known dimensions.

The fellowship work has focused on controlling the residual charge on the Au nanoparticle cores and developing mixed-valent films exhibiting higher conductivity than neutral counterparts. MPCs have the classical structure of a concentric sphere capacitor; a conductor (Au core) surrounded by a dielectric medium (alkanethiolate chains). This structure, along with extremely small Au core sizes, typically around 1.6 nm in diameter, enables sequential one-electron capacitive charging of the MPCs in solution.[3] Figure 2 (bottom) shows the differential pulse voltammogram (DPV) of the MPCs used for this study. Every one-electron MPC charging step can be regarded as a "redox" transformation with a pseudo-formal potential $E^{o'}$. At the current peak potentials, equal concentrations of a charge state "couple" (like $MPC^0$ and $MPC^{1+}$) exist at the electrolyte/electrode interface. At other potentials, relative concentrations of the charge state "couple" can be calculated using the Nernst equation. To produce large samples of

$$E-E^{0'} = 0.059 \log \frac{[MPC^{z+1}]}{[MPC^{z}]} \qquad [1]$$

mixed-valent MPCs a chemical charging method of emulsifying $Au_{140}C6_{53}$ (average composition) MPCs in $CH_2Cl_2$ with aqueous $Ce(SO_4)_2$ oxidizing solutions was developed. Once MPCs are re-collected from these mixtures, rest potential measurements yield E values that can be compared directly to the DPV $E^{o'}$ values allowing calculation of the ratio of charge states from Eq. 1 (shapes along the DPV are rest potentials of individually chemically charged MPC solutions as shown in Fig. 2).

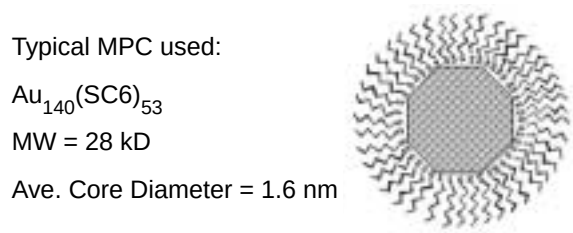


*FIG. 1. Schematic of a Monolayer Protected Gold Cluster (MPC).*

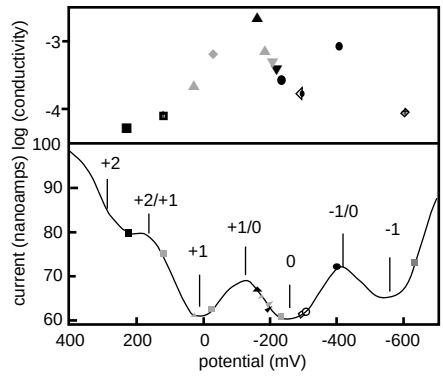


*FIG. 2. (top) 30°C electronic conductivity vs. rest potential (mV vs. $Ag/Ag^+$) of the solution from which the solid-state mixed valent MPC film was cast; (bottom) Differential pulse voltammogram (DPV) of a 96 μM $Au_{140}$(hexanethiolate)$_{53}$/ 0.1 M tetraoctylammonium bromide in $CH_2Cl_2$/0.6 mm Pt working electrode/non-aqueous ($Ag/Ag^+$ 0.01 M $AgNO_3$ reference/Pt coil counter. The shapes along the DPV trace are solution rest potentials of various chemically charged MPC solutions ($CH_2Cl_2$). The assignment of charge states (i.e. Z/Z+1) were assigned by the Nernst equation.*

The ratio of charge states in the solid-state is the same as in the MPC solutions. Several mixed-valent nanoparticle films were drop-cast from these characterized solutions and showed that film conductivity is a bimolecular process maximized when a 1:1 mix of Z and Z+1 charge states is approached. Figure 2 (top) shows room temperature conductivity as a function of rest potential of the various mixed-valent films prepared—the trend is clear. Equation 2[4] describes the bimolecular rate constant, $k_{EX}$,

$$k_{EX} = \frac{6RT\sigma_{EL}}{10^{-3}F^2\delta^2[MPC^{z}][MPC^{z+1}]} \qquad [2]$$

where $\sigma_{EL}$ is the conductivity, F is the Faraday constant, δ is the Au core-to-core distance (determined by pycnometry). $k_{EX}$ values for the 0/1+ and 0/1- mixtures of MPCs all fell in the 1-4 x $10^{10}$ $M^{-1}s^{-1}$ range. Once higher Au core charge states, such as 1+/2+ and 1-/2-, were obtained, lower $k_{EX}$ values around $10^8$ to $10^9$ $M^{-1}s^{-1}$ were calculated, indicating either a change in rate or mechanism. These rates indicate an extremely fast electron transfer between Au cores, in fact larger than expected when compared to Marcus theory predictions of non-adiabatic electron transfer.[5] The behavior is analogous to conductivity in doped semiconductor materials.

## Acknowledgments

The author would like to acknowledge The Electrochemical Society for the Edward G. Weston Summer Research Fellowship, and Professor Royce Murray for guidance in this project.

## References

1. M. Brust, M. Walker, D. Bethel, D. J. Schiffrin, and R. J. Whyman, *J. Chem. Commun.*, 801 (1994).
2. W. P. Wuelfing, S. J. Green, D. E. Cliffel, J. J. Pietron, and R. W. Murray, submitted (2000).
3. J. F. Hicks, A. C. Templeton, S. Chen, K. M. Sheran, R. Jasti, and R. W. Murray, *Anal. Chem.*, **71,** 3703 (1999).
4. R. H. Terrill, J. E. Hutchinson, and R. W. Murray, *J. Phys. Chem. B*, **101,** 1535 (1997).
5. R. A. Marcus, and N. Sutin, *Biochim. Biophys. Acta*, **811,** 265 (1985).

## About the Author

***Peter Wuelfing*** *is a graduate student at the University of North Carolina at Chapel Hill working for Professor Royce W. Murray.*

# Surface Studies of Spontaneously Deposited Ruthenium on Pt(hk) Electrodes

*A Summary Report to The Electrochemical Society for the 2000 Colin Garfield Fink Summer Research Fellowship*

**by Alechia Crown**

Recently, there has been an increased interest in the surface morphology of platinum-based catalysts, especially in reference to fuel-cell based research. In this area, a wide array of research is currently being conducted, as revealed by recent review articles.[1,2] Of urgent interest is the development and characterization of "poison-tolerant" catalysts. In the Direct Methanol Fuel Cell (DMFC), for example, there are a number of aspects keeping the technology from being highly efficient, one of which is catalytic inefficiency. Current theory suggests that platinum, ruthenium, and osmium constitute the most promising catalysts for the DMFC;[3-5] therefore, our research has focused on first the individual Pt/Ru and Pt/Os systems,[6] in an attempt to understand the enhancement effects of Ru and Os on the Pt catalyst.

Depositing controlled amounts of ruthenium onto well-defined surfaces (*e.g.,* Pt(hkl) electrodes), allows the study of surface structure effects in Pt/Ru methanol oxidation electro-catalysis. The deposits are spontaneously formed by placing the electrode in a hydrated $RuCl_3$ solution, where $RuO^{2+}$ species adsorb onto the platinum surface. After a brief voltammetric treatment, the species are reduced to form strongly adhered ruthenium islands; these islands are incredibly stable in the voltammetric region below platinum oxidation, which makes them ideal surfaces to explore by scanning tunneling microscopy (STM). It was determined previously that the Pt(111) surface covered by ruthenium yields the highest activity toward methanol electro-oxidation.[7] Herrero *et al.* determined that on Pt(111), spontaneously deposited Ru islands form three-dimensional structures, even at low Ru coverage.[8] Here, we explored the deposition process using *ex-situ* STM on Pt(111), Pt(100) and Pt(110). The ruthenium was deposited onto the surfaces using the electroless method, and Ru coverage values were obtained on the electrodes at various deposition times. These Ru coverage values give us an insight into the surface dynamics of the Ru island formation, especially with regard to surface site preference.

Figure 1 shows three images obtained on Pt(111), Pt(100) and Pt(110) after various deposition exposure times to a 5 mM $RuCl_3$ in .1 M $HClO_4$ solution. On all three surfaces, it is observed that the island deposition occurs homogenously across the surface, without regard to surface steps and planes.

Figure 1a is an image obtained on the 111 crystal after 40 seconds of deposition time. The average coverage value obtained was .14 ML, with an average island size of 3.4 nm. Exploring the bi-layer characteristics, it is observed that the ruthenium nucleation has an optimum island size, beyond which further nucleation does not occur, rather identical islands propagate along the surface, in addition to forming a second layer. Analysis of the imaging after 40 seconds for the bi-layer ruthenium features revealed that indeed approximately 8% of the islands show bi-layer characteristics.

Figure 1b is an image obtained on Pt(100) after only 20 seconds of deposition. The surface coverage value of Ru is also 0.14 ML. It was observed on Pt(100) that Ru islands tend to nucleate at a faster rate than on Pt(111), although this crystal face as well shows homogenous island formation, with the island size slightly similar to those on the 111 surface, with an average size of 3.5 nm. After 20 seconds, the bi-layer structures include 6% of the base ruthenium coverage.

Figure 1c is an image obtained on Pt(110) after 40 seconds of exposure to $RuCl_3$. This surface displayed the lowest "growth rate" of Ru adisland formation, as after 40 seconds of deposition, only .06 ML coverage was observed. The islands on this surface, like the previous two, also show homogeneous coverage and similar

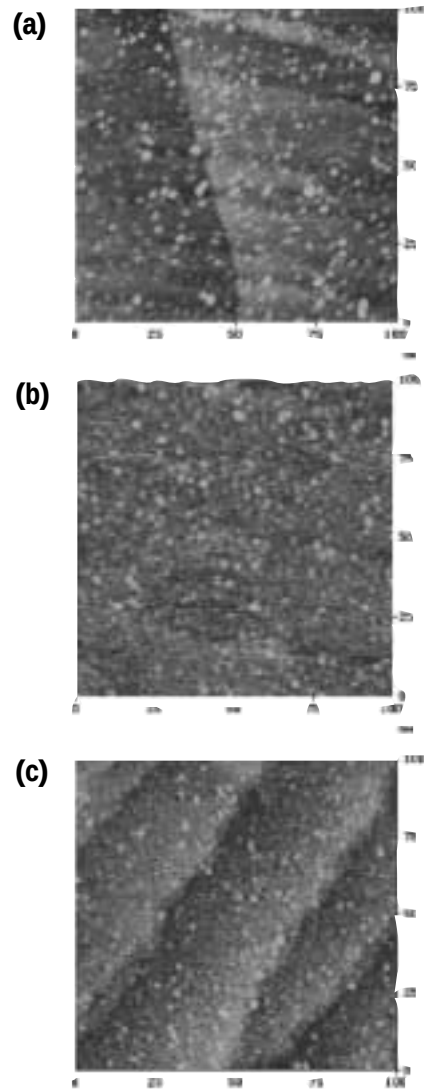


*FIG. 1. (a) STM image obtained on Pt(111) after 40 Ru deposition, coverage was 0.14 ML; (b) STM image obtained on Pt(100) after 20 Ru deposition, the coverage calculated is .14 ML; (c) STM image obtained on Pt(110) after 40 Ru deposition, the coverage value obtained is .06 ML. The images were obtained at 100 mV bias, and on a DI Multimode AFM/STM, equipped with a 10 micron scanner.*

**Table I.**

| Deposition Time, s | Pt(111) $\theta_{Ru}$, ML | Pt(100) $\theta_{Ru}$, ML | Pt(110) $\theta_{Ru}$, ML |
|---|---|---|---|
| 10 | .02 +/- .01 | .07 +/- .02 | .03 +/- .01 |
| 20 | .09 +/- .03 | .14 +/- .04 | .04 +/- .01 |
| 40 | .14 +/- .03 | .16 +/- .05 | .06 +/- .02 |
| 90 | .17 +/- .03 | .21 +/- .03 | .07 +/- .03 |
| 150 | .19 +/- .03 | .21 +/- .02 | .10 +/- .03 |

island size (3.5 nm average) and, like the other surfaces under study, the bilayer growth seemed to only occur on the larger (2 $nm^2$ or higher) islands.

Table I summarizes the coverage results obtained by STM for the surface index planes studied, and indicates that the spontaneous deposition of ruthenium is most effective on Pt(100), followed by Pt(111) and then by Pt(110). Further experiments including *in-situ* scanning probe methods, X-ray photoelectron spectroscopy, as well as electrochemical characterization, will additionally elucidate the deposition process and aid in the fundamental understanding of the ruthenium enhancement. These experiments studying the reactivity at noble metal electrodes may add to progress in electrochemistry, surface science, and materials science. ■

## Acknowledgments

The support by The Electrochemical Society through the Colin Garfield Fink summer fellowship is gratefully acknowledged. Professor Andrzej Wieckowski has aided tremendously in the advancement of this work, and the encouragement is much appreciated. This work was also supported by the National Science Foundation grant no. CHE 97-000963 and by the Department of Energy grant no. DEFG02-96ER45439 as administered by the Fredrick Seitz Materials Research Laboratory.

## References

1. D. T. Mah, J. W. Weidner, and S. Motupally, *J. Electrochem. Soc.*, **146**, 3924 (1999).
2. S. Wasmus and A. Kuver, *J. Electroanal. Chem.*, **461**, 14 (1999).
3. B. Beden, J.-M. Léger, and C. Lamy, in *Modern Aspects of Electrochemistry,* **Vol. 22** (J. O'M. Bockris, R. E. White, and B. E. Conway, eds.), p. 97, Plenum Press, New York (1992).
4. B. Gurau, R. Viswanathan, R. X. Liu, T. J. Lafrenz, K. L. Ley, E. S. Smotkin, E. Reddington, A. Sapienza, B. C. Chan, T. E. Mallouk, and S. Sarangapani, *J. Phys. Chem. B,* **102**, 9997 (1998).
5. E. Reddington, A. Sapienza, B. Gurau, R. Viswanathan, S. Sarangapani, E. S. Smotkin, and T. E. Mallouk, *Science,* **280,** 1735 (1998).
6. A. Crown, H. Kim, G. Q. Lu, I. R. Moraes, C. Rice, and A. Wieckowski, *J. New Mat. Electrochem. Sys.,* **3,** 275 (2000).
7. W. Chrzanowski and A. Wieckowski, *Langmuir,* **14**, 1967 (1998).
8. E. Herrero, J. M. Feliu, and A. Wieckowski, *Langmuir,* **15,** 4944 (1999).

## About the Author

***Alechia Crown*** *is a fourth year graduate student at the University of Illinois at Urbana-Champaign under the direction of Andrzej Wieckowski working toward her PhD in analytical chemistry.*

# Scanning Electrochemical Microscopy of Individual Living Cells

*A Summary Report to The Electrochemical Society for the 2000 Joseph W. Richards Summer Research Fellowship*

**by Biao Liu**

Reduction-oxidation reactions are among the processes essential for many cellular functions. Intracellular redox activity can be probed noninvasively by measuring the rate of transmembrane charge transfer (CT).[1] Previous measurements of interfacial redox activity typically employed large cell populations.[1] Measurements with ultramicroelectrodes made at the level of a single cell are much faster and provide valuable information that is hard to extract from the averaged signal produced by a large number of cells. The present work suggests the possibilities of measuring the rate and investigating the pathway of transmembrane charge transfer with the scanning electrochemical microscope (SECM).

In an SECM experiment, a micrometer-sized ultramicroelectrode (UME) is placed in solution containing the oxidized (or reduced) form of a redox mediator. A mediator species is then reduced (or oxidized) at the tip electrode. If the tip is positioned near an electrically conductive substrate, the product of the tip reaction diffuses to its surface, where it may be re-oxidized (or re-reduced). This process produces an enhancement in the faradaic current at the tip electrode depending on the tip/substrate separation distance (d). The overall rate of mediator regeneration at the substrate can be evaluated from the tip current-distance ($i_T$ - d) curve.[2] We used this approach to measure the rate of CT across the membrane of an individual cell.

Three cell lines were used in our experiments: (1) non-transformed, non-tumorigenic human breast epithelial cells (MCF-10A); (2) MCF-10A cells that were genetically engineered to overexpress PKCα (11α cells); and (3) metastic human breast cancer cells (MDA-MB-231), which also express high levels of PKCα. PKCα is an enzyme that has been mechanistically linked with cell adhesion and motility, two critical elements of metastasis.[3]

The $i_T$ vs. d curve obtained with a tip approaching the plastic surface of the culture dish (curve 1, Fig. 1), fits the theory for a diffusion-controlled process with an insulating substrate (solid line). When the same tip approached an MDA-MB-231 cell (metastatic cell) (curve 2), the $i_T$ was higher, indicating that the mediator was regenerated by the cell at a measurable rate. The effective heterogeneous rate constant, k = 1.4 x $10^{-3}$ cm/s, was obtained by fitting this curve to the SECM theory (solid line). The tip current for a MCF-10A cell (curve 4) was significantly higher than the $i_T$ obtained for a MDA-MB-231 cell (curve 2), resulting in k = 7 x $10^{-3}$ cm/s. Thus, a non-metastatic cell regenerates menadione at a significantly higher rate than does a metastatic cell. For an 11α cell, the rate constant (k = 2.4 x $10^{-3}$ cm/s from curve 3) was slightly higher than the k value for an MDA-MB-231 cell, but significantly lower than that for a MCF-10A cell. The slower mediator regeneration rates observed for 11α and MDA-MB-231 cells may be related to a high level of PKCα expression, a common factor in these cell lines.[4]

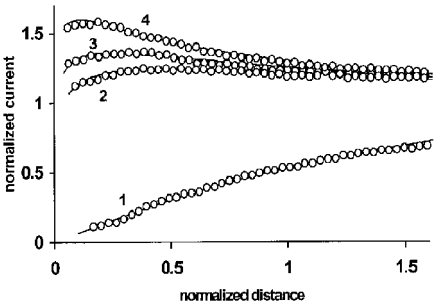


*FIG. 1. A 5.5-µm-radius carbon tip approaches (1) plastic surface, (2) MDA-MB-231 cell, (3) 11α cell, and (4) MCF-10A cell. Phosphate buffer (pH 7.4) contained 30 µM 1,2-naphthoquinone.*

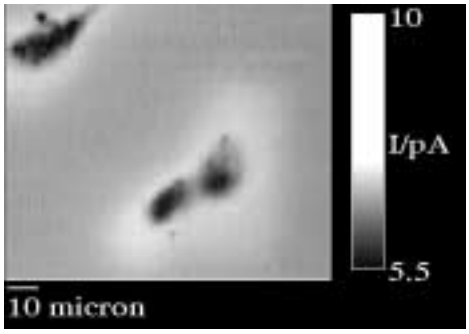


*FIG. 2. Normal human breast (MCF-10A) cells imaged by SECM with a 1-µm-radius Pt tip and 40 µM 1,2-naphthoquinone as mediator.*

SECM can also be used for electrochemical mapping of redox activity in an individual cell. An image (Fig. 2) was obtained using 40 µM 1,2-naphthoquinone as mediator for two aggregating MCF-10A cells and a neighboring cell. The bright halo at the cell periphery signifies the region of highest redox activity. A dark, redox inactive area in the center of the cell is a nucleus that is impenetrable to the mediator species.

In conclusion, SECM has been shown a suitable tool for probing CT reactions in single biological cells. Significant differences are detected in the redox responses given by non-transformed human breast epithelial cells and highly metastatic breast cancer cells. ■

## Acknowledgments

The author wishes to acknowledge his mentor, Prof. Michael V. Mirkin, for guidance and encouragement. Financial support from The Electrochemical Society Joseph W. Richards Summer Research Fellowship is also acknowledged.

## References

1. J. D. Rabinowitz, J. F. Vacchino, C. Beeson, and H. M. McConnell, *J. Am. Chem. Soc.*, **120**, 2464 (1998).
2. A. J. Bard, F.-R. F. Fan, and M. V. Mirkin, in *Electroanalytical Chemistry*, **Vol. 18,** ed. A. J. Bard, p. 243, Marcel Dekker, New York (1994).
3. S. P. Palecek, J. C. Loftus, M. H. Ginsberg, D. A. Lauffenburger, and A. F. Horwitz, *Nature*, **385,** 537 (1997).
4. X.-g. Sun and S. A. Rotenberg, *Cell Growth & Diff.*, **10,** 343 (1999).

## About the Author

***Biao Liu*** *is currently pursuing a PhD in chemistry at the City University of New York, under the direction of Prof. Michael V. Mirkin.*

# Electrochemical Molecular Beams

*A Summary Report to The Electrochemical Society for the 2000 Department of Energy Summer Research Fellowship*

**by Kyle M. Grant**

In the present report, I introduce a technique for focusing electrochemically generated molecules in solution using an external magnetic field. The acceleration of charge-carrying ions in an applied field is due to the generation of a magnetic body force. This force per volume ($N/m^3$) is given by Eq. 1, where J ($C\ m^{-2}\ s^{-1}$) is the flux of

$$F_{vol} = J \times B \qquad [1]$$

ions, and B (T) is the applied field.[1] The transfer of momentum from the accelerated ions to the solvent gives rise to magnetohydrodynamic (MHD) flow of electrolytic solution.[2,3]

For single-electrode systems, the magnetic force can significantly alter the rate of mass transport to the electrode surface.[4-6] When a dual-electrode configuration is employed, induced flow patterns create a unique molecular transport system. The dual-electrode configuration, used to transport focused ions, is shown in Fig. 1. Two Pt inlaid microdisk electrodes (radius = 250 µm) are at facing angles of 0° and 180°, with respect to the applied field. Both microelectrodes are poised at a potential of -2.0 V (*vs.* $Ag/Ag_xO$), in an acetonitrile solution containing 2 M nitrobenzene (NB). NB radical anion generated at the electrodes is dark red and easily imaged by video microscopy. When a uniform magnetic field of 1.0 T is applied, the magnetic force induces a rotational flow of solution at the circumference of one microelectrode. Mass conservation requires an inward flow to balance the outward flow at the inlaid disk edge. The inward flow is a tightly focused beam and can transport the NB anion over distances up to 1.0 cm at velocities of ~0.25 cm/s. The direction of the beam can be varied by changing the positions of the microelectrodes. Molecules can also be focused into other geometrical shapes, *e.g.*, 1 cm diameter, 50 µm wide circular sheets.

The ion beam has been investigated electrochemically by employing a microelectrode probe, positioned to move through the MHD flow pattern. The probe, indicated by the arrow in Fig. 1, is fabricated by electropolymerization of a polyphenol insulating coating onto a 25 µm radius Pt wire.[7] The end of the insulated wire is cut to expose a disk shape electrode. The probe is poised at a potential (0.0 V *vs.* $Ag/Ag_xO$) to oxidize the electrogenerated NB radical anions. Figure 2 shows a plot of current *vs.* distance as the probe is moved through a cross section of an ion beam. A rough estimate of the ion beam diameter (~75 µm) can be obtained from this profile. The scatter in the current is due to flow instabilities.

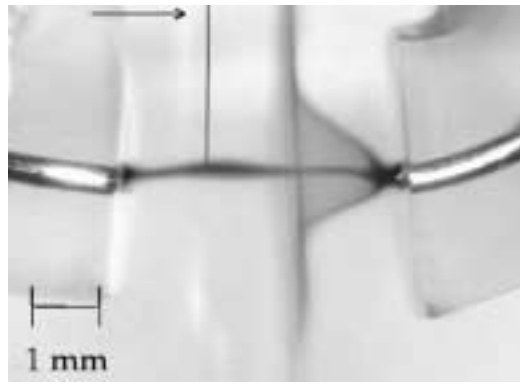


*FIG. 1. Video micrograph of the transport of nitrobenzene anion in a tightly focused beam, between two Pt microdisk electrodes. A microelectrode probe positioned within the ion beam is indicated by the arrow.*

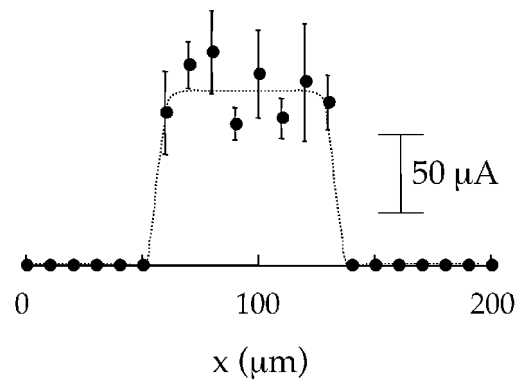


*FIG. 2. Plot of the microelectrode probe current vs. distance as the tip is moved through a molecular beam.*

The present work shows that molecules can be focused into molecular ion beams and transported over macroscopic distances in an electrochemical system, without the aid of mechanical devices or channels to direct solution flow. Future investigations into the applications of this technique may prove useful in chemical analysis and in solution-phase microfabrication. ■

## Acknowledgments

I would like to thank The Electrochemical Society for the Department of Energy Research Fellowship to support this summer research. I would also like to gratefully acknowledge the Office of Naval Research for their support of this project and Dr. Henry S. White for his guidance.

## References

1. D. J. Griffiths, *Introduction to Electrodynamics, 3rd Ed.*, Prentice Hall: Upper Saddle River, NJ (1999).
2. T. Z. Fahidy, *Modern Aspects of Electrochemistry,* **Num. 32,** Kluwer Academic, New York, NY (1999).
3. S. R. Ragsdale and H. S. White, *Anal. Chem.*, **71,** 1923 (1999).
4. N. Leventis, M. Chen, X. Gao, M. Canalas, and P. Zhang, *J. Phys Chem. B,* **102,** 3512 (1998).
5. S. R. Ragsdale, J. Lee, X. Gao, and H. S. White, *J. Phys. Chem.*, **100,** 5913 (1996).
6. S. R. Ragsdale, K. M. Grant, and H. S. White, *J. Am. Chem. Soc.*, **120,** 13461 (1998).
7. K. Potje-Kamloth, J. Janata, and M. Josowicz, *Ber. Bunsenges. Phys. Chem.*, **93,** 1480 (1989).

### About the Author

***Kyle M. Grant*** *is an ECS student member. He is currently a graduate student of analytical chemistry at the University of Utah.*

# Chemical Investigations of the GaAs to Borosilicate Glass Wafer Bonded Interface

*A Summary Report to The Electrochemical Society for the 2000 Department of Energy Summer Research Fellowship*

**by Darren M. Hansen**

Wafer bonding is the process of contacting two flat, smooth, and chemically compatible surfaces to form a bond across the interface. To a large extent, studies of the bonding process have focused on the use of $SiO_2$ and Si that have been treated to produce hydrophilic surfaces.[1] In this case, the bond that forms across the interface involves hydrogen bonded $H_2O$ and OH groups at room temperature that evolve during high temperature annealing to covalent Si-O bonds.[2] The use of doped oxides, such as $xB_2O_3 \cdot SiO_2$ (BSG), and different semiconductors, such as GaAs, provides even greater flexibility in engineering the properties of the resulting bonded structure. For example, the $B_2O_3$ content in a borosilicate glass (BSG) controls the viscosity and thermal expansion coefficient (TEC) of the bonding medium. BSG has been investigated in the development of a glass-bonded compliant substrate.[3] The fabrication of these structures for wafer bonding or compliant substrate applications would be enhanced by a detailed knowledge of the chemistry occurring at the semiconductor-to-BSG wafer bonded interface.

The interfacial chemistry of the GaAs-to-BSG coated GaAs bonded wafer pair was probed by multiple internal transmission Fourier transform infrared (MIT-FTIR) spectroscopy.[2] In this technique, polarized light is introduced into a beveled edge of bonded sample, schematically shown in Fig. 1, transmitted through the bonded interface several times, and detected after exiting the sample. This technique has been used with great success in probing the chemistry of the Si wafer bonded interface.[2]

Figure 2 provides a MIT-FTIR spectrum for a room temperature bonded GaAs-to-BSG-coated GaAs bonded sample. In this case, 30 mole % $B_2O_3$-70 mole % $SiO_2$ was deposited by low-pressure chemical vapor deposition.[3] As shown in Fig. 2, the $H_2O$/OH peak intensities at 1,670 $cm^{-1}$ and 3,000-3,600 $cm^{-1}$ are strong for the as-bonded sample, indicating the presence of water at the room temperature bond.[2] In addition, peaks at 800 and 900 $cm^{-1}$ are also present in the as-bonded sample indicating the presence of Ga-O and As(III)-O vibrations.[4,5] The presence of Ga-O and As(III)-O vibrations have been confirmed by comparison to GaAs-to-GaAs bonded samples with no oxide present (not shown).


*FIG. 1. Schematic of the MIT-FTIR geometry showing the multiple passes through the bonded interface (shown for clarity in gray). The measurement entails two polarizations of light termed the p- and s-polarizations. The diagram shows the geometry of the electric field vector relative to the sample surface for each polarization.*

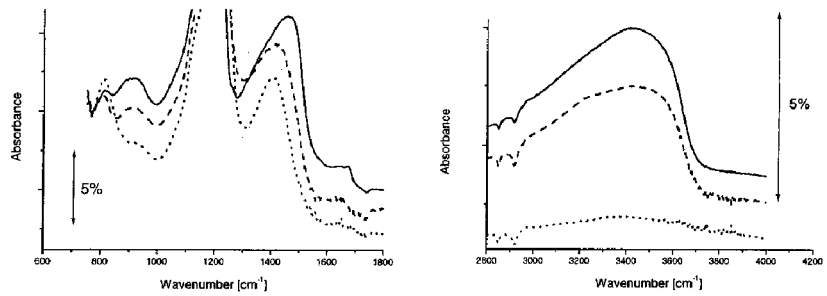


*FIG. 2. MIT-FTIR spectra for GaAs-to-$(SiO_2)_{0.7}(B_2O_3)_{0.3}$/GaAs wafer bonded samples after various anneals in $N_2$ for 1 hour. (—) is for the as-bonded spectra. (---) is for a sample annealed at 300°C. (…) is for a sample annealed at 600°C. The primary $SiO_2$ peak between 1,100-1,200 $cm^{-1}$ is cut off and peaks are offset for clarity. These spectra are a composite of the p- and s-polarized spectra for the samples following a modified procedure as described in reference 2.*

Thermal annealing in $N_2$ strengthens the bond, causing the bonding chemistry to evolve. Figure 2 also provides spectra for bonded samples annealed at 300°C and 600°C. The peak at 900 $cm^{-1}$, attributed to As(III)-O vibrations, decreases, while the peak at 800 $cm^{-1}$ increases. This observation is consistent with previous reports that As(III)-O are thermodynamically unstable and decompose, resulting in the formation of Ga-O.[6] The water peaks decreases with increasing annealing temperature indicating a removal of the $H_2O$ and OH groups in favor of other covalent bonds at the interface. The bonding chemistry investigations also suggest the formation of As(V)-O, however, this observation requires further investigation.

The bonding chemistry of GaAs-to-BSG appears to involve the following sequence. Initially, the bond is made by hydrogen bonded $H_2O$ and OH groups similar to what is proposed for Si hydrophilic bonding.[2] As the bonded samples are annealed the oxides of As(III)-O are reduced and Ga-O bonds are formed while the $H_2O$ and OH groups are removed from the interface. Finally, after a high temperature annealing step, the bonded interface consists of covalently bonded oxides consisting of Si-O, B-O, Ga-O and possibly As(V)-O species. ■

## Acknowledgments

The author wishes to acknowledge the financial support of the DOE Summer Research Fellowship from The Electrochemical Society. Funding from the ONR-MURI on Compliant Substrates and facilities support from the NSF UW-MRSEC is gratefully acknowledged. Guidance and encouragement from the author's advisor, Professor T. F. Kuech, was invaluable to the success of this project.

## References

1. See references cited in the following: *Semiconductor Wafer Bonding: Science, Technology and Applications I*, U. Gösele, T. Abe, J. Haisma, and M. A. Schmidt, Editors,

*(continued on next page)*

## Hansen

*(continued from previous page)*

PV 92-7, The Electrochemical Society Proceedings Series, Pennington, NJ (1992); *Semiconductor Wafer Bonding: Science, Technology and Applications II*, M. A. Schmidt, T. Abe, C. E. Hunt, and H. Baumgart, Editors, PV 93-29, The Electrochemical Society Proceedings Series, Pennington, NJ (1993); *Semiconductor Wafer Bonding: Science, Technology and Applications III*, C. E. Hunt, H. Baumgart, S. S. Iyer, T. Abe, and U. Gösele, Editors, PV 95-7, The Electrochemical Society Proceedings Series, Pennington, NJ (1995).

2. M. K. Weldon, V. E. Marsico, Y. J. Chabal, D. R. Hamann, S. B. Christman, and E. E. Chaban, *Surface Science*, **368,** 163 (1996).
3. D. M. Hansen, P. D. Moran, K. A. Dunn, S. E. Babcock, R. J. Matyi, and T. F. Kuech, *J. Cryst. Growth*, **195**, 144 (1998).
4. C. C. Bahr, A. vom Flede, and M. J. Cardillo, *J. Electron. Spectroscopy and Related Phenomena*, **54/55**, 1075 (1990).
5. E. S. Aydil, Z. Zhou, K. P. Giapis, Y. Chabal, J. A. Gregus, and R. A. Gottscho, *Appl. Phys. Lett.*, **62,** 3156 (1993).
6. G. P. Schwartz, G. J. Gualtieri, J. E. Griffiths, and B. Schwartz, *J. Electrochem. Soc.*, **128,** 410 (1981).

### About the Author

***Darren M. Hansen*** *is currently pursuing his PhD in chemical engineering at the University of Wisconsin-Madison under the supervision of Professor T. F. Kuech. His thesis entitled, "Low-Pressure Chemical Vapor Deposition of Borosilicate Glasses for Materials Integration Applications", is planned to be completed in the spring of 2001.*

# The Electrochemistry of an Al-Zn-Mg-Cu Alloy in Simulated Crack-Tip Solutions

*A Summary Report to The Electrochemical Society for the 2000 Department of Energy Summer Research Fellowship*

**by Kevin R. Cooper**

Mechanistic understanding of intergranular (IG) environment-assisted cracking (EAC) of Al-Zn-Mg-Cu alloys in aqueous chloride solutions is lacking in part because the crack-tip electrode kinetics are not well known. The objective of this work was to characterize the alloy electrode kinetics in simulated crack-tip solutions. This work is part of a larger study examining the crack chemistry and electrochemistry of aluminum association (AA) 7050 to help elucidate the relative contribution hydrogen embrittlement (HE) and anodic dissolution (AD) to the crack advance process.[1-3] The crack chemistry and electrode potential have been described.[4-7]

## Experimental

The electrochemical behavior of AA 7050 was examined in simulated crack-tip solutions using standard potentiodynamic techniques.[8] Factorial experimental design and analysis[9] were used to statistically determine the effects of $Al^{3+}$, $Cl^-$, and $Cr^{6+}$ concentration and pH (Table I) on the anodic and cathodic kinetics of bulk alloy material and analogs representing phases relevant to the IG cracking phenomenon: alloy matrix, precipitate free zone (PFZ) and grain boundary intermetallic $MgZn_2$ and $Mg(Zn,Cu,Al)_2$.[10] Statistical tests were conducted at a significance level of $\alpha = 0.05$.

**Table I. Factor levels for 1/2 fractional factorial analysis.**

| Level | $Al^{3+}$, M | $Cl^-$, M | $Cr^{6+}$, M | pH |
|---|---|---|---|---|
| Low | 0.017 | 0.05 | 0.5 | 3.5 |
| High | 0.25 | 0.5 | 2.5 | 2.5 |

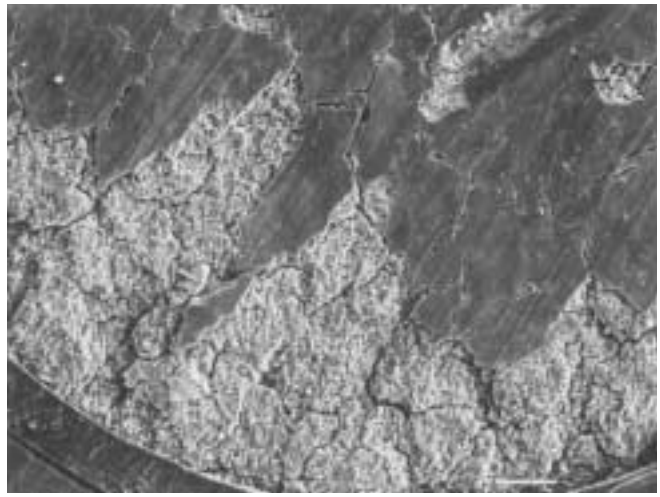

*FIG. 1. Intergranular corrosion of AA 7050-T651 observed in 0.25 M $Al_2(Cr_2O_7)_3$ + 0.5 M NaCl + 1.0 M $Cr^{6+}$ as $Al_2(Cr_2O_7)_3$ + $CrO_3$ + $Na_2CrO_4$, pH 3.5, deaerated. 1200 grit finish, scan rate = 0.167 mV/sec.*

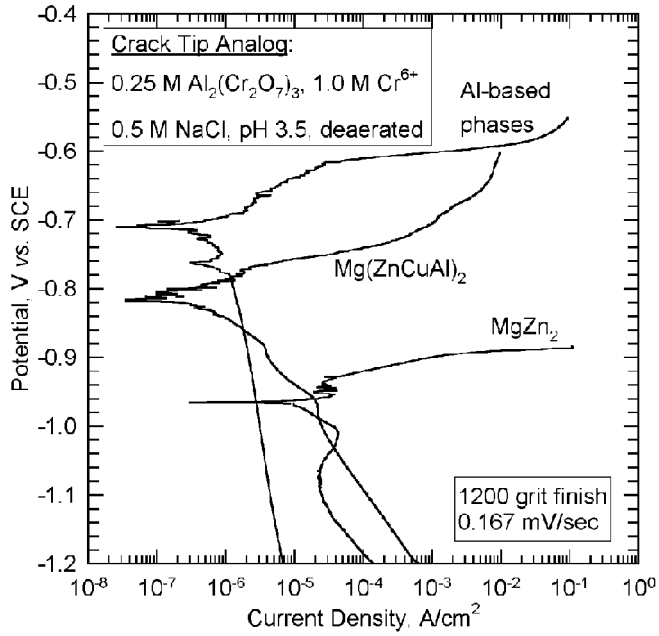


*FIG. 2. Electrochemical behavior of Al-Zn-Mg-Cu alloy phases in simulated crack-tip solution.*

## Results and Conclusions

Understanding the crack-tip electrode kinetics is of primary importance to understanding the EAC-mechanism of Al-Zn-Mg-Cu alloys. Although both T651 and T7451 material exhibited pitting at their free corrosion potential ($E_{corr}$) and on anodic polarization in a crack-tip simulate, EAC-susceptible T651 suffered severe IG corrosion (Figure 1) where as T7451 material did not. The excellent EAC-resistance of the latter may in part be due to its enhanced grain boundary corrosion resistance.[11,12]

Figure 2 summarizes the electrochemical behavior of the bulk and analog materials in a crack-tip simulate. Aluminum-based electrodes (*i.e.*, bulk T651 and T7451, matrix and PFZ analogs) were susceptible to localized attack at their free corrosion potential ($E_{corr}$) in the acidic, high [$Cl^-$] environments; both intermetallics exhibited general dissolution, were active relative to the Al-based materials, and exhibited enhanced dissolution and reduction kinetics relative to the Al materials. Note that incorporation of Al and Cu into the intermetallic reduces the galvanic difference between the grain boundary particles and surrounding PFZ and matrix.

Statistical analysis revealed that within the factor ranges studied, increasing [$Al^{3+}$] or [$Cl^-$] or reducing [$Cr^{6+}$] decreased $E_{corr}$ of AA 7050-T651; none of the factors had a statistically

significant effect on the corrosion current density ($i_{corr}$). Increasing $[Al^{3+}]$ or $[Cr^{6+}]$ or pH decreased $E_{corr}$ of $MgZn_2$. With increasing $[Al^{3+}]$ or acidity, $i_{corr}$ for $MgZn_2$ increased.

Bare metal dissolution, repassivation and hydrogen reduction kinetics and H-uptake in crack tip analog solutions will be examined using the scratched electrode technique[13] to simulate crack tip film rupture events.

## Acknowledgments

The Electrochemical Society's Student Summer Fellowship funded this work. Additional financial support from the Alcoa Foundation is gratefully acknowledged. The author also acknowledges the technical support of his PhD advisor Prof. R. G. Kelly and undergraduate research assistant J. W. Pak of the University of Virginia.

## References

1. N. J. H. Holroyd, in *Environment-Induced Cracking of Metals,* **Vol. 10**, R. P. Gangloff and M. B. Ives, eds., NACE, Houston TX (1990), p. 311.
2. M. O. Speidel, in *Hydrogen Embrittlement and Stress Corrosion Cracking,* R. Gibala and R. F. Hehemann, eds., ASM Intl., Metals Park, OH, (1984), p. 271.
3. T. D. Burleigh, *Corr.,* **47,** 89 (1991).
4. K. R. Cooper, R. G. Kelly, and E. L. Colvin, *Corrosion/99 Paper No. 153,* NACE, Houston, TX (1999).
5. K. R. Cooper, and R. G. Kelly, *J. Chromatogr. A,* **850,** 381 (1999).
6. K. R. Cooper, L. M. Young, R. P. Gangloff, and R. G. Kelly., in *7th International Conference on Aluminum Alloys: Their Physical and Mechanical Properties,* **Vol. 3,** E. A. Starke, Jr., T. H. Sanders, Jr., and W. A. Cassada, eds., Trans Tech Publications, Enfield, NH (2000), p. 1625.
7. A. Turnbull, in *Proceedings of the Second International Conference on Localized Corrosion,* **Vol. 9,** H. S. Isaacs, U. Bertocci, J. Kruger, and S. Smialowska, eds., NACE, Houston TX (1990), p. 359.
8. *Metals Test Methods and Analytical Procedures,* **Vol. 3.02,** Wear and Erosion; Metal Corrosion, ASTM, Philadelphia, PA (1990), p. 77.
9. J. S. Milton and J. C. Arnold, *Introduction to Probability and Statistics: Principles and Applications of Engineering and the Computing Sciences,* McGraw-Hill, Inc., New York, NY (1995).
10. J. E. Hatch, *Aluminum: Properties and Physical Metallurgy,* ASM, Metals Park, OH, (1984).
11. P. Doig, P. E. J. Flewitt, and J. W. Edington, *Corr.,* **33,** 217 (1977).
12. B. Sarkar, M. Marek, and E. A. Starke, Jr., *Met. Trans. A,* **12A,** 1939 (1981).
13. R. C. Newman, in *Corrosion Chemistry Within Pits, Crevices and Cracks,* A. Turnbull, ed., HMSO, Teddington, Middlesex (1984), p. 317.

## About the Author

***Kevin R. Cooper*** *is a doctoral candidate and graduate research assistant at the Center for Electrochemical Science and Engineering, Department of Materials Science and Engineering at the University of Virginia. He is a student member of ECS.*

# Measuring Heterogeneous Electron Transfer Rates of Monolayer Protected Clusters

*A Summary Report to The Electrochemical Society for the 2000 Department of Energy Summer Research Fellowship*

**by Jocelyn F. Hicks**

Nanometer-sized metallic and semiconducting particles have been the focus of much research due to a heightened interest in these materials for potential applications such as molecular catalysts, chemical sensors, and optoelectronic devices.[1] To date, research on Monolayer Protected Clusters (MPCs) has yielded important insight on several fronts. One interesting observation is that the combination of a small metal-like core with a hydrocarbon dielectric coating (Fig. 1) makes MPCs minute capacitors, with capacitance values of less than one attofarad (aF) per particle in electrolyte solution. Addition or removal of individual electrons from the core of these tiny capacitors produce potential changes $\Delta V = e/C_{CLU} > k_BT/e$. This has led to the exciting observation that MPCs exhibit quantized double layer (QDL) capacitive charging in electrolyte solution.[2] Recently we have also shown that MPCs functionalized with carboxylic acids exhibit QDL charging in solution as well as when they are attached to an electrode surface through a series of carboxylate metal linkages[3] (Fig. 2).

This summer, I have focused on measuring the heterogeneous electron transfer rate (kET) between the electrode and an MPC tethered to the electrode surface. Cyclic voltammograms display QDL charging peaks, making it possible to use the technique made familiar by Laviron[4] to estimate kET. I hypothesize that electron transfer occurs by the electron tunneling from the electrode surface through the monolayer to the MPC. Marcus theory predicts that the reorganizational energy barrier ($\lambda_o$) to electron transfer will be small owing to the non-polar dielectric surrounding the core, and therefore the rate of electron transfer will be fast. Attaching the MPC to the electrode surface via a hydrocarbon chain slows kET and permits the use of standard electrochemical techniques in measuring the electron transfer rate.

The peak current ($E_P$) in the cyclic voltammogram is proportional to scan rate ($\nu$) as is expected for a surface confined redox species (Fig. 3). The slope of a plot of $E_P$ versus ln $\nu$ is equal to $-2.3RT/\alpha nF$, where $\alpha$ is the transfer coefficient. After determining $\alpha$ we can use Eq. 1 to estimate $k_{ET}$

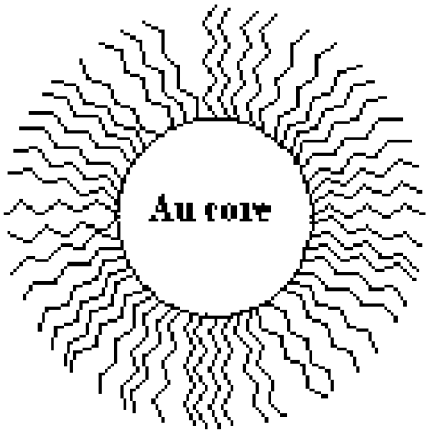


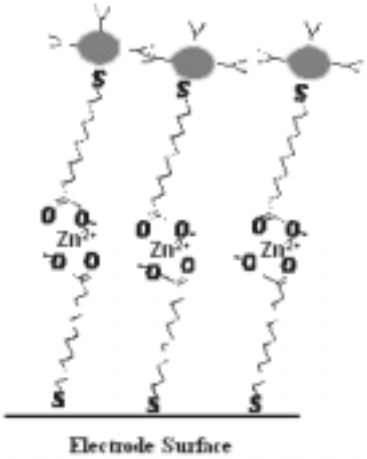


*FIG. 1. (above left) Schematic of a monolayer protected gold cluster.*

*FIG. 2. (above right) Schematic of hexanethiolate MPCs each functionalized with ca. 5 mercaptoundecanoic acid ligands attached to a gold electrode surface through $Zn^{2+}$ metal carboxylate bonds.*

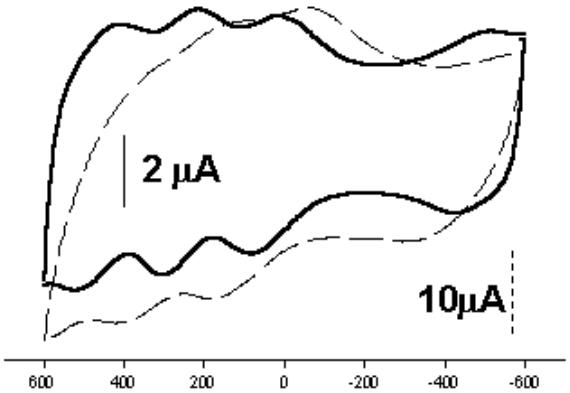


*FIG. 3. (bottom right) Cyclic Volmammetry (CV) showing the dependence of peak potential ($E_p$) of surface confined MPC on scan rate (v). (-) v = 50 mV/s (---) v= 22 Vs.*

$$\log k_{ET} = \alpha\log(1-\alpha) + (1-\alpha)\log\alpha - \log(RT/nFn) - \alpha(1-\alpha)nF\Delta E_P/2.3RT \quad [1]$$

I estimated a rate of 45 $s^{-1}$ using cyclic voltammetry. This is slightly faster than predicted for a ferrocene molecule attached to the electrode through an alkane chain of similar length.[5]

The work described here applies a known electrochemical technique to a new class of materials, and provides fundamental information about their electrochemistry. Continued studies will be aimed at understanding factors influencing $k_{ET}$, such as the dielectric constant and the length of the monolayer. ■

## Acknowledgments

The author would like to thank The Electrochemical Society and the Department of Energy for funding this work through a summer fellowship. This work was also supported in part by grants from NSF and ONR.

## References

1. (a) M. A. Hayat, Ed., *Colloidal Gold: Principles, Methods and Applications*, **Vol. 1**, Academic Press, New York (1989); (b) G. Schmid, Ed., *Clusters and Colloids*, VCH, Wienheim (1994).
2. (a) R. S. Ingram, M. J. Hostetler, R. W. Murray, T. G. Schaaff, J. T. Khoury, R. L. Whetten, T. P. Bigioni, D. K. Guthrie, and P. N. First, *J. Am. Chem. Soc.*, **119**, 9279 (1997); (b) J. F. Hicks, A. C. Templeton, S. Chen, K. M. Sheran, R. Jasti, R. W. Murray, J. Debord, T. G. Schaaff, and R. L. Whetten, *Anal. Chem.*, **71**, 3703, (1999).
3. F. P. Zamborini, J. F. Hicks, and R. W. Murray, *J. Am. Chem. Soc.*, **122**, 4514 (2000).
4. E. Laviron, *J. Electroanal. Chem.*, **101**, 19 (1979).
5. J. F. Smalley, S. W. Feldberg, C. E. D. Chidsey, M. R. Linford, M. D. Newton, and Y-P. Liu, *J. Phys. Chem.*, **99**, 13141 (1995).

## About the Author

***Jocelyn Hicks** is a graduate student at the University of North Carolina at Chapel Hill studying under Professor Royce W. Murray.*

# Catalytic Reduction of $O_2$ to $H_2O$ by Vanadium-Schiff Base Complexes in Acetonitrile

*A Summary Report to The Electrochemical Society for the 2000 Department of Energy Summer Research Fellowship*

**by Zenghe Liu**

Four-electron reduction of $O_2$ to $H_2O$ in organic solvents is difficult. In a recent report,[1] we demonstrated the potential of the vanadium(III) complex of salen ($H_2$salen = N,N'-ethylenebis(salicylideneamine)), $V^{III}(salen)^+$, as a catalyst for the reduction of $O_2$ to $H_2O$ in acidified acetonitrile. The novelty of the chemistry involved in the catalysis and the likelihood that it could also be applied to the electroreduction of $O_2$ provided impetus for an expanded study of analogous vanadium complexes. Thus, a variety of oxovanadium complexes with different Schiff base ligands, $V^{IV}O(SB)$ (SB = Schiff base), were prepared and characterized spectroscopically and electrochemically.[2] In Table I are listed those complexes with sufficient solubility in acetonitrile to allow solution studies to be carried out. These complexes were found to disproportionate rapidly and quantitatively upon reaction with strong acids (such as $HClO_4$ and $CF_3SO_3H$) according to reaction 1:

$$2V^{IV}O(SB) + 2H^+ \longrightarrow V^{V}O(SB)^+ + V^{III}(SB)^+ + H_2O \qquad [1]$$

All the $V^{III}(SB)^+$ complexes produced in reaction 1 were found to accomplish the stoichiometric and quantitative reduction of $O_2$ according to reaction 2:

$$V^{III}(SB)^+ + O_2 \longrightarrow V^{V}O(SB)^+ \qquad [2]$$

Since $V^{V}O(SB)^+$, the product of reaction 2, can be reduced either chemically or electrochemically to $V^{IV}O(SB)$, a catalytic reduction of $O_2$ proceeds in the presence of excess acid. The rate of the catalytic cycle was found to be limited by the rate of reaction 2.

A general and efficient approach for the preparation of $V^{III}(SB)^+$ complexes was developed. It involves the reductive deoxygenation of the readily available $V^{IV}O(SB)$ with $H_2$ in the presence of a large area platinum gauze (on which $H_2$ is dissociatively adsorbed). The $V^{III}(SB)^+$ formed in this way was used to monitor the kinetics of reaction 2 using a carbon microelectrode held at a potential where the oxidation of $V^{III}(SB)^+$ was diffusion limited. The data obtained showed that the rate of reaction 2 was first-order in both $V^{III}(SB)^+$ and $O_2$. A possible mechanism for the reaction is given in reactions 3-5:

**Table I. Structures of $V^{IV}O(SB)$ complexes and rate constants of the oxidation of the corresponding $V^{III}(SB)^+$ complexes by $O_2$.**

| No. | $R_1$ | $R_2$ | $R_3$ | $R_4$ | X | $k_3$($M^{-1}$ $s^{-1}$) |
|---|---|---|---|---|---|---|
| 0 | H | H | H | H | $CH_2CH_2$ | 0.06 |
| 1 | t-Bu | H | t-Bu | H | $CH_2CH_2$ | 0.44 |
| 2 | H | H | H | H | 1,2-$C_6H_4$ | 0.06 |
| 3 | t-Bu | H | t-Bu | H | 1,2-$C_6H_4$ | 0.46 |
| 4 | H | H | MeO | H | $CH_2CH_2$ | 0.13 |
| 5 | H | MeO | H | MeO | $CH_2CH_2$ | 0.11 |

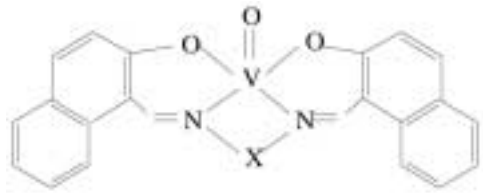

| | | | | | | |
|---|---|---|---|---|---|---|
| 6 | | | | | 1,2-$C_6H_4$ | 0.09 |

$$V^{III}(SB)^+ + O_2 \underset{k_{-3}}{\overset{k_3}{\rightleftharpoons}} (SB)VO_2^+ \qquad [3]$$

$$(SB)VO_2^+ + V^{III}(SB)^+ \xrightarrow{k_4} (SB)VOOV(SB)^{2+} \qquad [4]$$

$$(SB)VOOV(SB)^{2+} \xrightarrow{k_5} 2V^{V}O(SB)^+ \qquad [5]$$

The corresponding rate law when the steady-state approximation is applied and $k_{-3} << k_4$ is :

$$-\frac{d[V^{III}(SB)^+]}{dt} = 2k_3[V^{III}(SB)^+][O_2]$$

Values of $k_3$ were evaluated for several complexes as listed in Table I. The rate constants span the range of 0.06 to 0.46 $M^{-1}$ $s^{-1}$. A distinctive feature of this mechanism is that the rate-determining step is the formation of an intermediate, $(SB)VO_2^+$, that probably requires the dissociation of a solvent molecule from an axial position on the $V^{III}(SB)^+$ complex to generate a coordination site for the incoming $O_2$ molecule. Much higher rates of reaction 4 and 5 are believed to result in the observed, quantitative formation of $V^{V}O(SB)^+$. The larger rate constants exhibited by complexes 1 and 3 (Table I) might be attributed to the four bulky tertiary butyl groups which increase the lability of solvent molecules coordinated to the axial sites on the $V^{III}(SB)^+$ complexes.

## Acknowledgment

The author would like to thank Professor Fred C. Anson for his guidance and encouragement. The Energy Research Summer Fellowship from The Electrochemical Society, Inc., and financial support from the National Science Foundation are also gratefully acknowledged.

## References

1. Z. Liu and F. C. Anson, *Inorg. Chem.*, **39,** 274 (2000); *Inorg. Chem.* **39**, 1048 (2000).
2. Z. Liu and F. C. Anson, *Inorg. Chem.*, in press.

## About the Author

***Zenghe Liu*** *is currently pursuing a PhD in chemistry at the California Institute of Technology under the direction of Professor Fred C. Anson.*